AIP | The Journal of Chemical Physics

Resolution-of-identity stochastic time-dependent configuration interaction for dissipative electron dynamics in strong fields

Stefan Klinkusch and Jean Christophe Tremblay

Citation: The Journal of Chemical Physics **144**, 184108 (2016); doi: 10.1063/1.4948646
View online: http://dx.doi.org/10.1063/1.4948646
View Table of Contents: http://scitation.aip.org/content/aip/journal/jcp/144/18?ver=pdfcov
Published by the AIP Publishing

Resolution-of-identity stochastic time-dependent configuration interaction for dissipative electron dynamics in strong fields

Stefan Klinkusch and Jean Christophe Tremblay
Institute for Chemistry and Biochemistry, Freie Universität Berlin, Takustr. 3, D-14195 Berlin, Germany

(Received 8 February 2016; accepted 24 April 2016; published online 11 May 2016)

In this contribution, we introduce a method for simulating dissipative, ultrafast many-electron dynamics in intense laser fields. The method is based on the norm-conserving stochastic unraveling of the dissipative Liouville-von Neumann equation in its Lindblad form. The N-electron wave functions sampling the density matrix are represented in the basis of singly excited configuration state functions. The interaction with an external laser field is treated variationally and the response of the electronic density is included to all orders in this basis. The coupling to an external environment is included via relaxation operators inducing transition between the configuration state functions. Single electron ionization is represented by irreversible transition operators from the ionizing states to an auxiliary continuum state. The method finds its efficiency in the representation of the operators in the interaction picture, where the resolution-of-identity is used to reduce the size of the Hamiltonian eigenstate basis. The zeroth-order eigenstates can be obtained either at the configuration interaction singles level or from a time-dependent density functional theory reference calculation. The latter offers an alternative to explicitly time-dependent density functional theory which has the advantage of remaining strictly valid for strong field excitations while improving the description of the correlation as compared to configuration interaction singles. The method is tested on a well-characterized toy system, the excitation of the low-lying charge transfer state in LiCN. *Published by AIP Publishing.* [http://dx.doi.org/10.1063/1.4948646]

I. INTRODUCTION

Ultrafast electron dynamics in intense laser fields is a topic of increasing experimental importance.[1–9] Understanding the transient behavior of electrons on their natural time scale is central to, e.g., predicting spectroscopic properties of molecules. Electronic excitations have already been used to induce nuclear rearrangements and to observe chemical reactions. As first demonstrated in Zewail's seminal experiments,[10,11] many electronic processes occur on a femtosecond (fs, 1 fs = 10^{-15} s) time scale. In recent years, the attosecond (as, 1 as = 10^{-18} s) barrier has been breached,[12,13] providing a wealth of experimental information that requires careful theoretical analysis.

From a theoretical perspective, great progress has been made over the last decade in the description of ultrafast electron dynamics.[14–49] A popular solution is offered by the explicitly time-dependent density functional theory (TDDFT).[50] Despite its computational efficiency and transparent interpretation, it was shown to suffer from shortcomings when dealing with strong field excitations,[51,52] where non-linear effects can lead to false absorption spectra, while some workarounds have been proposed.[53] On the other hand, wave function based approaches such as time-dependent Hartree-Fock (HF)[14] and multi-configuration time-dependent Hartree-Fock[25,26,30] appear promising in that respect despite the obvious drawback stemming from the exponential scaling.

Our method of choice builds on the configuration interaction (CI) methodology,[54,55] which was recently extended and applied to the explicitly time-dependent case.[23,31,41,42,56–61] In the time-dependent configuration interaction (TDCI) method, the CI eigenstates calculated at a given level (CI Singles, CI Doubles, etc.) are used as a dynamical basis to represent and to propagate the N-electron wave function. The major limitation of this method is its high computational cost, restricting the description of electron correlation to at most perturbative doubles for medium-sized molecular systems. Fortunately, the physics of many interesting ultrafast processes is dictated by single excitations. As was recognized by Sonk and Schlegel,[62] TDCI only requires the energies of the system eigenstates and the associated transition dipole moments, which can be directly obtained also from linear response time-dependent density functional theory. The physics of the electron dynamics can thus be interpreted in terms of single excitations, while alternative choices of density functional can yield a better treatment of electron correlation. In this DFT-based TDCI formalism, spurious non-linear effects from TDDFT are alleviated at the cost of using a very large dynamical basis of eigenstates. Computing a large number of N-electron eigenstates represents an important bottleneck of the method and can rapidly become intractable for medium-size systems.

To allow investigation of larger systems, we introduced a reduced density matrix variant[63] of the TDCI method building on a system-bath separation, which we dubbed ρ-TDCI.[40,45,64,65] In this approach, only the explicit evolution of the electron density matrix of the relevant part of the system embedded in the surrounding environments is considered explicitly, leading to a reduced-dimensionality dissipative-type dynamics. The method was extended to treat ionizing

systems using a heuristic one-electron rate model,[45] in which the loss of norm in the electron density is interpreted as the time-dependent ionization probability. To reduce the computational cost associated with storing and propagating the density matrix, a dissipative system can alternatively be treated using stochastic wave function approaches.[66–73] The evolution of the reduced density matrix is sampled by a collection of wave functions evolving according to stochastic differential equations. These define a probability distribution on Hilbert space, which yields an estimate of the reduced density matrix upon incoherent averaging.[72,74] To ensure that the waiting-time distribution are sampled properly, the scheme requires that the stochastic wave packets remain normalized at all times.

In this contribution, we propose a norm-conserving stochastic propagation scheme for simulating N-electron dynamics of dissipative, ionizing systems based on the time-dependent configuration interaction formalism. The stochastic wave packets are represented in a complete basis of configuration state functions, which yields the most accurate variational description possible of the field-matter interaction. In the interaction picture, the exponential of the Hamiltonian operator describing the coherent dynamics of the system at all times is treated using the resolution-of-identity approximation. This allows to reduce significantly the size of the eigenstate basis required for the dynamical simulation while not compromising the linear variational description of the laser-molecule interaction. Ionization is mediated by transition operators to an auxiliary state belonging to the ionized continuum at a rate determined by a modified kinematic one-electron model. The method retains the desirable properties of the TDCI method and satisfies the norm-conserving requirement of Monte Carlo wave packet methods.[75]

This paper is organized as follows: In Sec. II, the stochastic TDCI scheme is presented. In Sec. III, the method is benchmarked using LiCN as a test system. Sec. IV summarizes the properties of the method. Unless stated otherwise, atomic units are used throughout the paper ($\hbar = m_e = e = 4\pi\varepsilon_0 = 1$). They are, however, sometimes mentioned for clarity.

II. THEORY

A. Stochastic density matrix for dissipative *N*-electron dynamics

The reduced density matrix (RDM) formalism is a potentially very efficient tool to study laser-induced many-electron dynamics for systems in contact with an environment. The evolution of the RDM operator associated with an N-electron system, $\hat{\rho}(t)$, obeys the Liouville-von Neumann equation

$$\frac{\partial\hat{\rho}(t)}{\partial t} = -i[\hat{H}(t),\hat{\rho}(t)] + \hat{\hat{\mathcal{L}}}_D\hat{\rho}(t), \tag{1}$$

where $\hat{\hat{\mathcal{L}}}_D$ is the dissipative Liouvillian. The first term on the right-hand-side describes the coherent evolution of the system under the influence of the time-dependent Hamiltonian, $\hat{H}(t)$. For the simulation of laser-driven excitations, it is convenient to write the time-dependent Hamiltonian in the interaction picture, which in the semi-classical dipole approximation reads

$$\hat{H}(t) = -e^{+i\hat{H}_{el}t/\hbar}\hat{\mu}\underline{F}(t)e^{-i\hat{H}_{el}t/\hbar}. \tag{2}$$

The dipole operator is defined as $\hat{\mu} = -\sum_i^N er_i + \sum_A^{N_A} Z_A eR_A$, and $\underline{F}(t)$ denotes a time-dependent external electric field. The field-free electronic Hamiltonian $\hat{H}_{el}$ for a system composed of N electrons and N_A nuclei can be written in the clamped nuclei approximation as

$$\hat{H}_{el} = -\frac{1}{2}\sum_{i=1}^{N}\nabla_i^2 - \sum_{i=1}^{N}\sum_{A=1}^{N_A}\frac{Z_A}{r_{iA}} + \sum_{i=1}^{N}\sum_{j>i}^{N}\frac{1}{r_{ij}}, \tag{3}$$

where r_{ij} is the distance between the electrons i and j, and r_{iA} is the distance between the electron i and the nucleus A with charge Z_A. The last term in Eq. (1) is a Liouvillian superoperator $\hat{\hat{\mathcal{L}}}_D$ describing the dissipation of the energy and phase in the system due to its contact with the surroundings. The latter remains in thermal equilibrium at all times and its influence on the system dynamics can be revealed, e.g., by tracing out the associated degrees of freedom from the equations of motion of the total system+bath.[75] It will be shown in Section II C how it can also be used to describe photoionization processes.

The evolution of the RDM can be conveniently simulated from incoherent averaging over an ensemble of N_{tr} wave functions

$$\hat{\rho}(t) = \frac{1}{N_{tr}}\sum_{j=1}^{N_{tr}}\Psi_j(t)\Psi_j^*(t). \tag{4}$$

Each quantum trajectory $\Psi_j(t)$ evolves according to a stochastic Schrödinger equation (SSE), which usually takes either the form of a quantum jump process[67,70,73–75] or of quantum state diffusion.[66,71] Propagation of the stochastic density matrix (SDM) alleviates its explicit storage and scales linearly with the number of considered trajectories, i.e., $N_{tr}N_{tot}^2$ for stochastic wave packets of length N_{tot}, compared to N_{tot}^3 for the explicit RDM. If the number of stochastic wave functions to characterize the statistical behavior of the RDM is smaller than the size of the basis, the computational cost of such the SDM propagation can be reduced significantly.

For Markovian dynamics, the system can be understood as following a piecewise deterministic evolution, with occasional random jumps that are induced by coupling to the environment (see, e.g., Ref. 75 and references therein). In this formal unravelling of the Lindblad master equation, a swarm of wave functions is incremented over a short time interval dt by independent stochastic equations

$$|d\Psi_j(t)\rangle = -\frac{i}{\hbar}\left(\hat{H}_{NL}(t) + \frac{i\hbar}{2}\sum_k \gamma_k\|\hat{C}_k|\Psi_j(t)\rangle\|^2\right)|\Psi_j(t)\rangle dt + \sum_k\left(\frac{\hat{C}_k|\Psi_j\rangle}{\|\hat{C}_k|\Psi_j(t)\rangle\|^2} - |\Psi_j(t)\rangle\right)d\xi_k(t). \tag{5}$$

Here, $\hat{C}_k$ is a so-called Lindblad operator representing the kth dissipative channel with rate γ_k. The Poisson increment $d\xi_k(t)$ must satisfy the relations

$$d\xi_j(t)d\xi_k(t) = \delta_{jk}d\xi_k(t),$$
$$\mathrm{E}[d\xi_k(t)] = \gamma_k\|\hat{C}_k|\Psi_j(t)\rangle\|^2 dt. \quad (6)$$

The first line describes the fact the stochastic processes are independent (i.e., uncorrelated) and $\mathrm{E}[d\xi_k(t)]$ stands for the expectation value of the Poisson increment. The non-linear operator $\hat{H}_{NL}$ is defined by the field-free Hamiltonian in the interaction representation (Eq. (2)) and the operators $\hat{C}_k$, i.e.,

$$\hat{H}_{NL}(t) = -e^{+i\hat{H}_{el}t/\hbar}\hat{\mu}\underline{F}e^{-i\hat{H}_{el}t/\hbar} - \frac{i\hbar}{2}\sum_k \gamma_k\hat{C}_k^\dagger\hat{C}_k. \quad (7)$$

In the following, the first term on the right-hand-side will be labeled "coherent," as opposed to the term $\frac{i\hbar}{2}\sum_k \gamma_k\hat{C}_k^\dagger\hat{C}_k$ representing incoherent dissipation. In an efficient implementation of Eq. (5), each wave function follows a deterministic evolution driven by the Hamiltonian $\hat{H}_{NL}$ (Eq. (7)) leading to a loss of norm in the wave packet that can be related to the waiting time distribution before a jump occurs in the quantum trajectory.[75] This loss of norm is then compared to a random number, in order to decide if a certain trajectory undergoes such an event (relaxation, excitation, photoionization, etc.). In the next step, the wave function is either renormalized (if no jump occurred) or jumps to a statistically selected random state. This approach is sometimes called the Monte Carlo wave packet method and is described in more detail elsewhere.[74] In the limit of $N_{tr} \to \infty$, the stochastic density matrix reproduces exactly the Markovian evolution of the RDM following the Liouville-von Neumann equation in its Lindblad form.[75]

B. The resolution-of-identity stochastic time-dependent configuration interaction (RI-sTDCI) method

In this work, the dissipative many-electron dynamics is described within the time-dependent configuration interaction framework. In its original formulation,[23,40] the TDCI method represents the RDM operator in the basis of approximate eigenfunctions of the field-free Hamiltonian, although alternate basis representations have been also proposed for wave packet dynamics.[76,77] The solutions of the time-independent Hamiltonian, Eq. (3), are obtained as linear combinations of spin-adapted excited Slater determinants, or configuration state functions (CSFs). The excited CSFs are typically constructed from a reference Hartree-Fock calculation for the ground state of Eq. (3) and aim at systematically and variationally build in correlation in the N-electron eigenstates. The correlated eigenstates obtained by diagonalization of the Hamiltonian matrix at a chosen level of theory (CI Singles, CI Doubles, . . ., Full CI) are then used as the dynamical basis. CI can be in principle improved systematically, although these expansions can rapidly become prohibitively expensive.

The variational convergence of laser-molecule interaction Hamiltonian Eq. (7) can be very slow in strong electric fields. For this reason, a large number of CI eigenstates are required in the TDCI expansion, which comes at the cost of computing matrix elements of the field-free Hamiltonian (Eq. (3)), followed by a costly diagonalization. To ensure variational convergence of the field-molecule interaction while reducing the computational cost associated with generating the dynamical basis, the Hamiltonian (Eq. (2)) can be alternatively represented in the basis of singly excited configuration state functions. For a molecule in a given spin state σ, the jth time-dependent stochastic CIS wave packets can be defined as

$$\Psi_j^{(\sigma)}(t) = D_{0,j}(t)\Psi_0^{(\sigma)} + \sum_{a\in\mathrm{occ.}}\sum_{r\in\mathrm{virt.}} D_{a,j}^r(t)\Psi_a^{r,(\sigma)}, \quad (8)$$

with $\{D_{0,j}(t), D_{a,j}^r(t)\}$ as the expansion coefficients and $\{\Psi_0^{(\sigma)}; \Psi_a^{r,(\sigma)}\}$ as the configuration space functions (CSFs).[78] This choice of basis is sufficient to describe the physics of all one-electron dynamical processes, while providing only an approximate description of correlation. In this basis, the coherent part of the time-dependent Hamiltonian matrix takes the form

$$\underline{\underline{H}}(t) = -\sum_{q=x,y,z} F_q(t)\exp\left(i\underline{\underline{H}}_{el}t\right)\underline{\underline{\mu}}^{(q)}\exp\left(-i\underline{\underline{H}}_{el}t\right), \quad (9)$$

where $\underline{\underline{\mu}}^{(q)}$ denotes the qth component of the dipole moment matrix, which can be trivially computed in the CSF basis using the Slater-Condon rules. Since the total number of CSFs can become intractable, computational saving is obtained by inserting an incomplete, yet sufficiently large set of auxiliary functions in Eq. (9)

$$\underline{\underline{H}}(t) \simeq -\sum_{q=x,y,z} F_q(t)\,\underline{\underline{U}}\,\underline{\underline{U}}^\dagger\exp\left(i\underline{\underline{H}}_{el}t\right)\underline{\underline{U}}\,\underline{\underline{U}}^\dagger\underline{\underline{\mu}}^{(q)}$$
$$\times\underline{\underline{U}}\,\underline{\underline{U}}^\dagger\exp\left(-i\underline{\underline{H}}_{el}t\right)\underline{\underline{U}}\,\underline{\underline{U}}^\dagger, \quad (10)$$

where $\underline{\underline{U}} = [\underline{u}_0, \underline{u}_2, \ldots, \underline{u}_M]$ is a rectangular matrix containing $M \leq N$ auxiliary vectors. This idea is sometimes called resolution-of-identity in the context of density fitting of electronic Coulomb integrals.[79–82] Here, the N-electron wave packets evolve mostly on the ground and other excited bound states. All excited states above IP ionize rapidly and are only involved in the coherent evolution of the N-electron system to mediate indirect coupling with the continuum via multi-photon excitations. Accordingly, the low-lying eigenstates supported by the field-free Hamiltonian, $\underline{\underline{H}}_{el}\underline{u}_m = E_m\underline{u}_m$, up to a given energy cutoff are expected to capture the physics of the coherent dynamics up to this energy. Note that any other subset of eigenvectors could be used to describe higher quasi-resonant excitations. The evaluation of the propagator is also simplified in this basis, as the exponential terms become diagonal, i.e.,

$$\underline{\underline{H}}(t) \simeq -\sum_{q=x,y,z} F_q(t)\,\underline{\underline{U}}\exp\left(i\underline{\underline{E}}_{el}t\right)\underline{\underline{U}}^\dagger\underline{\underline{\mu}}^{(q)}\underline{\underline{U}}$$
$$\times\exp\left(-i\underline{\underline{E}}_{el}t\right)\underline{\underline{U}}^\dagger, \quad (11)$$

where $\underline{\underline{E}}_{el}$ is an $M\times M$ diagonal matrix of the energies associated with the M lowest-lying eigenstates of the field-free Hamiltonian. Propagation of a wave function requires the application of the Hamiltonian matrix appearing in Eq. (11) on a vector representing the state of the system at time t. Provided the product of each matrix on a vector of dimension N_{tot} is performed sequentially, the operation of the

propagator in Eq. (11) thus scales as $4N_{tot} \times M + 2M^2 + N_{tot}^2$. This products thus scales roughly as $\sim N_{tot}^2$ since the CSF basis is generally much larger than the auxiliary eigenstate basis. In Section III, it will be shown that great computational savings can be expected from the resolution-of-identity without compromising the quality of the dynamical simulations.

A great advantage of the proposed method is that it can construct the TDCI propagator solely from the output of any quantum chemistry program, as only the energies of selected eigenstates and the associated eigenvectors are required. The latter are necessary to compute the dipole moment matrix in Eq. (11). Since CI Singles offers only a minimal description of electron correlation, it can be useful to investigate alternative quantum chemical methods to include correlation in the wave functions without departing from the single excitation picture, as was already recognized by others.[62] Hence, we propose computing the energies of excited states using linear response time-dependent density functional theory and extract the associated eigenfunctions from a correspondence principle based on the Tamm-Dancoff approximation. By doing so, the matrix elements of the dipole matrix can be computed as in the CI Singles method while propagator, Eq. (11), remains unchanged. This procedure gives access to a wide range of exchange-correlation functionals that can be chosen to improve the quality of the excitation spectrum, based on conventional knowledge on their performance for a given type of system.

C. Treatment of dissipation and photoionization

As discussed in Section II A, the stochastic propagator, Eq. (7), can be used to represent Markovian dissipative dynamics of the Lindblad type. The dissipative Liouvillian in parent equation, Eq. (1), takes the form

$$\hat{\hat{\mathcal{L}}}_D\hat{\rho}(t) = -\frac{1}{2}\sum_k([\hat{C}_k\hat{\rho}(t),\hat{C}_k^\dagger] + [\hat{C}_k,\hat{\rho}(t)\hat{C}_k^\dagger]), \quad (12)$$

where the Lindblad operators $\hat{C}_k$ can be used to mediate various physical processes. The Lindblad semigroup formalism ensures semi-positivity of the reduced density matrix operator and enables probabilistic interpretation of its diagonal elements as populations of the zeroth order states used for its representation.

In the RI-sTDCI method, energy excitation/relaxation induced by contact with the environment is described using raising/lowering operators in the CSF basis

$$\hat{C}_k \rightarrow \sqrt{\gamma_{a,r\rightarrow b,s}}|\Psi_b^s\rangle\langle\Psi_a^r|, \quad (13)$$

where $\gamma_{a,r\rightarrow b,s}$ is the rate associated with population transfer from CSF Ψ_a^r to CSF Ψ_b^s. In the present work, we choose to calculate the relaxation rates using the so-called *Surface-enhanced Relaxation Approach* (SERA) model, which mimics the effect of an electron-rich environment on the local dynamics

$$\gamma_{a,r\rightarrow b,s} = 4n|\mu_{a,r\rightarrow b,s}^{tot}|^2\frac{|\omega_{a,r\rightarrow b,s}|^3}{3c_0^3}. \quad (14)$$

Here, $|\mu_{a,r\rightarrow b,s}^{tot}|^2 = \sum_{q=x,y,z}(\mu_{a,r\rightarrow b,s}^q)^2$ is the total transition dipole moment, c_0 is the speed of light in vacuum, and $\hbar\omega_{a,r\rightarrow b,s} = (\varepsilon_s + \varepsilon_a - \varepsilon_r - \varepsilon_b)$ is the transition frequency between different configurations (ε_i is the energy of spatial orbital i). n is an effective refractive index ($n = 1$ for vacuum) used to scale the rates to typical time scales for metallic environments, on the order of a few to hundreds of femtoseconds. The excitation rates can be obtained from the relaxation rates via detailed balance, i.e., $\gamma_{a,r\rightarrow b,s} = \gamma_{a,r\leftarrow b,s}\ \exp(-\hbar\omega_{a,r\rightarrow b,s}/k_BT)$. Note that the toy system proposed here investigates an intramolecular charge transfer in an artificial electron-rich environment. The SERA model is introduced as an example and solely used to test the behaviour of the present methodology. The system is tailored so that ionization dominates over the energy relaxation channels.

Photoionization is treated in a similar way. In previous work, each zeroth order eigenstate of the field-free Hamiltonian was attributed a lifetime, computed from the CI Singles eigenfunctions and corresponding to a simple kinematic model describing the above-threshold ionization. This leads to a loss of norm in the RDM, which was interpreted as the ionization yield. This formulation is incompatible with the stochastic density matrix description proposed here, which requires renormalization of the wave packet at each time step (see Section II A). To circumvent this problem, an auxiliary state representing the ionization channel is added to the basis of configuration state functions, leading to a norm-conserving propagation scheme. This element does not undergo coherent evolution and is only accessible via an irreversible population transfer operator, which can be written in the Lindblad form $\hat{C}_k \rightarrow \sqrt{\Gamma_{a,r\rightarrow\mathcal{I}}}|\mathcal{I}\rangle\langle\Psi_a^r|$. The ionization rate for the ground state Hartree-Fock configuration is defined as zero, and so is the one associated with all transitions to bound orbitals defined according to Koopmans' theorem. For any other CSF an ionization rate is calculated analogously to the heuristic model developed by Klamroth and co-workers[42] according to

$$\Gamma_{a,r\rightarrow\mathcal{I}} = \begin{cases}\dfrac{\sqrt{\varepsilon_r}}{d}, & \text{if } \varepsilon_r > 0,\\ 0, & \text{else,}\end{cases} \quad (15)$$

where ε_r is the energy of the virtual orbital to be filled in this CSF. The rational behind this model is that the excess energy from the excitation to an unbound orbital is completely transferred to the kinetic energy of the electron. As in previous work,[42,45,62,83] the parameter d represents the escape length of the electron, at which it is irreversibly lost to the ionization continuum. Note that using the CSFs as the basis, a restriction ($\varepsilon_r > 0$) is only imposed on the electron in the excited orbital, while the second restriction to the ionization rate as in Klamroth's model ($E_n \geq IP$) is not applied. Within the RI-sTDCI method, all eigenstates of the system used in the resolution-of-identity expression for the propagator are considered stationary. It will be shown in Section III that the physical picture proposed by the two models concur with each other. Finally, an important difference to the model proposed by Rohringer *et al.*[84] for electron dynamics in strong optical laser fields is that all orbitals, configuration state functions,

and eigenstates used in the RI-sTDCI approach are real-valued. A similar non-unitary dynamics is obtained here by propagation using a non-unitary operator, which is defined in Eq. (11).

III. BENCHMARK CALCULATIONS: CHARGE TRANSFER DYNAMICS IN LICN

A. Static calculations

To benchmark the RI-sTDCI method, let us look at the charge transfer dynamics in a prototypical system, lithium cyanide (LiCN). All singlet states of a linear LiCN molecule in its equilibrium geometry, optimized at the restricted Hartree-Fock level of theory (R_{Li-C} = 3.683 a$_0$, R_{C-N} = 2.186 a$_0$), are computed without frozen core using a 6-31G* basis set[85] on all atoms. The excitation energies and associated wave functions are calculated with the GAMESS 07 program package[86] using either configuration interaction singles (CIS) or linear response time-dependent density functional theory (TDDFT). A total of N_{orb} = 45 orbitals (N_{occ} = 8 occupied and N_{virt} = 37 virtual) were used to generate singly configuration state functions from the reference, resulting in 297 excited singlet configuration state functions. For the TDDFT reference, different exchange-correlation functionals (namely, PBE,[87,88] CAM-B3LYP,[89] and B3LYP[90–92]) are used to assess the quality of the description of the charge transfer dynamics. The number of bound orbitals, defined from the orbital energies as $\varepsilon_r < 0$, is found to be N_b = 9 for CIS and CAM-B3LYP and N_b = 11 for PBE and B3LYP. The remaining orbitals are coupled to the continuum according to Eq. (15).

The energies of the low-lying eigenstates obtained with all four dynamical bases are shown in Fig. 1, along with the first ionization potential according to Koopmans' theorem.[93] As one can see, the fundamental gap decreases from CIS over CAM-B3LYP, B3LYP to PBE. This is expected because CIS tends to overestimate excitation energies, while pure density functionals such as PBE often underestimate excitation energies. The transition to the first charge transfer state to be used as a target in dynamical simulations (the second excited state or S_2) is indicated by the lower blue arrows in each case. The excitation corresponds mainly to an electron transfer from cyanide to lithium, i.e., $Li^+ CN^- \rightarrow (Li^0CN^0)^*$ and can be identified by visual inspection of the orbitals forming the dominant character of the depicted transitions. The lifetime of the target state is defined to be 66 fs according to the SERA model at the CIS level of theory. The transition energy decreases from $\hbar\omega_{0,2}$ = 0.2418 E$_h$ (6.58 eV) for CIS to $\hbar\omega_{0,2}$ = 0.1579 E$_h$ (4.30 eV) for PBE. For lack of experimental data, the EOM-CCSD transition frequencies are used as references. Among the time-dependent density functional methods, the CAM-B3LYP result (0.1958 E$_h$ or 5.33 eV) compared best to a reference EOM-CCSD calculation for the selected state (0.2306 E$_h$ or 6.28 eV), whereas the density of state is larger in the latter case than in any of the spectra presented in Fig. 1. Interestingly, the transition dipole moment obtained from the eigenstates is strong for CIS ($\mu^x_{0,2}$ = 0.3015 ea$_0$ (0.7663 D)) but significantly weaker for CAM-B3LYP ($\mu^y_{0,2}$ = 0.2323 ea$_0$ (0.5904 D)), PBE ($\mu^x_{0,2}$ = 0.2075 ea$_0$ (0.5274 D)), and B3LYP ($\mu^y_{0,2}$ = 0.1787 ea$_0$ (0.4542 D)). A weaker transition dipole moment implies that a higher electric field intensity will be required for laser induced excitation and will lead to a higher probability of multi-photon excitations. The sequential absorption of a second photon to quasi-resonant states originates from so-called dynamical broadening and is indicated by the upper blue arrows in Fig. 1. It leads to population of states located far above the ionization threshold, which rapidly decay to the continuum.

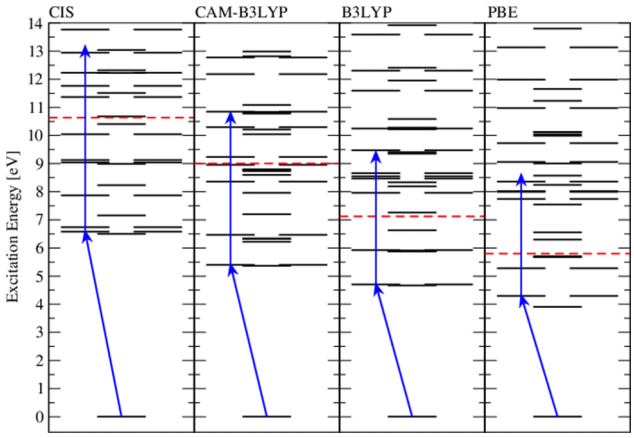

FIG. 1. Shown are the energy schemes for the lowest excited states in LiCN, using CIS (left panel), CAM-B3LYP (second panel), B3LYP (third panel), and PBE (right panel). All results are obtained at the optimized Hartree-Fock geometry, using the basis set 6-31G* on all atoms and without frozen core. The red dashed lines show the first ionization potential according to Koopmans' theorem. The blue arrows show the intended excitation (lower arrows) and a competing second absorption process (upper arrows).

The ionization rates computed using Eq. (15) depends on the orbital energies. Both Hartree-Fock ($-\varepsilon_{HOMO}$ = 0.3881E_h) and CAM-B3LYP ($-\varepsilon_{HOMO}$ = 0.3289E_h) yield physically sound values for the first ionization potential as compared to the energy difference between neutral and ionic ground states (ΔSCF = 0.3470E_h and ΔDFT = 0.3877E_h, respectively). On the contrary, PBE ($-\varepsilon_{HOMO}$ = 0.2133E_h vs. ΔDFT = 0.3710E_h) and B3LYP ($-\varepsilon_{HOMO}$ = 0.2619E_h vs. ΔDFT = 0.3788E_h) perform poorly. This is due to the incorrect asymptotic behaviour of the latter two functionals. In all cases, the ionization rates obtained from the orbital energies are at least one order of magnitude larger than the timescales of the excitation dynamics (circa 10 fs) and of energy relaxation (circa 50 fs). Consequently, their exact value will not affect the dynamics significantly. Their relative value is of importance to determine the preferred ionization channel, which will be the subject of future work.

B. Influence of the resolution-of-identity

An important aspect of the RI-sTDCI method is the definition of a small subset of eigenstates for which the coherent dynamics is described exactly. To evaluate how the resolution-of-identity affects the transient dynamics, the population evolution of selected states driven by an electric field is investigated for various sizes of the auxiliary eigenstate basis. An x-polarized laser field is chosen here as

$$\underline{F}(t) = \underline{f}(t)\cos(\omega(t-t_p)),$$
$$\underline{f}(t) = \begin{cases} \underline{f}_0 \cos^2\left(\frac{\pi(t-t_p)}{2\sigma}\right), & \text{if } |t-t_p| < \sigma, \\ 0, & \text{else.} \end{cases} \quad (16)$$

Here, $\underline{f}(t)$ is the time-dependent shape function of the pulse, consisting of a $\cos^2$ function and an amplitude $\underline{f}_0$, t_p is the time at the pulse maximum, and σ is the full width at half maximum (FWHM) of the pulse. Finally, ω is the carrier frequency of the laser pulse. Note that, by symmetry, similar results would be obtained with y-polarized pulses and, consequently, only the former simulations are presented. A first guess for the pulse parameters can be made from the π-pulse condition, tailored to a complete inversion of population in an idealized two-level system within the rotating wave approximation. The amplitude can be calculated from the transition dipole moment $\underline{\mu}_{f,i}$ and the FWHM as

$$\underline{f}_0 = \frac{\hbar\pi}{\sigma \underline{\mu}_{f,i}}. \quad (17)$$

In all simulations, the number of trajectories is set to 50, reasonable for both a proper description and a reduction of the computational cost, as compared to the full RDM propagation.

For lithium cyanide, there are two physically motivated basis sizes that can be used as references: the complete basis of 297 eigenstates, or a truncated eigenstate basis of 186 states corresponding to the frozen core approximation. In this first example, the latter is chosen for comparison of the population evolution. The π-pulse parameters for the charge transfer process are chosen resonant to the $S_0 \rightarrow S_2$ transition energy for the each method represented. For example, at the CIS level, these are: $\hbar\omega = 0.2418$ E_h (6.58 eV), $t_p = \sigma = 200$ $\frac{\hbar}{E_h}$ (4.84 fs), and $f_0^x = 5.21 \times 10^{-2}$ $\frac{E_h}{e a_0}$ (26.8 GV/m). The propagation ends at $t_f = 454.8$ $\frac{\hbar}{E_h}$ (11 fs), slightly after the pulse end to evaluate the effect of energy relaxation. The resulting populations for the ground state as the initial state, the second excited state as the target state, and the norm loss to the ionization continuum are shown in Fig. 2. As one can see, the temporal development of the populations is very similar in all cases, especially for the ground state and the target state. Due to the very short duration of the pulse and the comparatively long energy relaxation lifetime of the excited states according to the SERA model, no significant effect of energy relaxation is observed in the simulations. For the ground state population, the final value is found in a range between 0.10 and 0.15. While the final population for the 100 and 150 subsets approximately matches that of the reference subset with 186 states, it is found to be lower with 50 states. The final target state populations also behave similarly, where the resolution-of-identity with 50 states gives a slightly lower population at the end of the pulse than for the reference system. Consequently, the ion yields at the end of the propagation are seen to be slightly overestimated with the smallest auxiliary basis: ~0.70 for 150 and 100 states and 0.78 for 50 states, the reference resulting in an ionization yield of 0.72. This figure provides a first evidence that the original basis of 297 CSFs can be truncated to a subset with 100 auxiliary eigenstates without affecting the dynamics in the frozen core approximation, which a reduction down to 50 states would not even alter significantly.

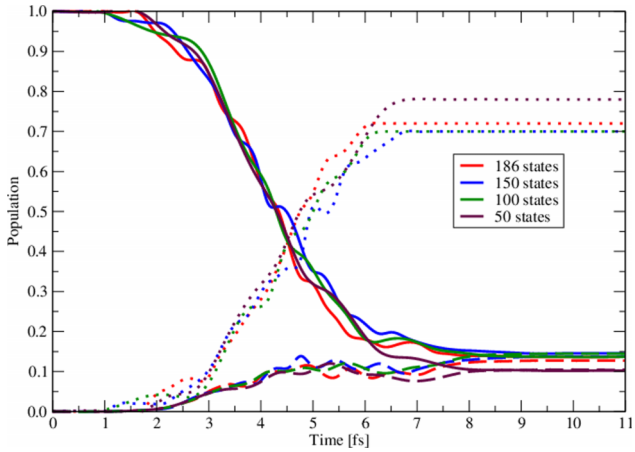

FIG. 2. Populations of the ground state (S_0, solid), the charge transfer state (S_2, dashed), and ionization continuum (Ion., dotted) for an RI-sTDCI simulation based on CIS results with 186 states (red), 150 states (blue), 100 states (green), and 50 states (maroon).

To evaluate the effect of the frozen core on the resolution-of-identity, Fig. 3 shows the final population of the two selected states (S_2, top panel, and S_0, central panel) and the ionization yield (bottom panel) as a function of the auxiliary basis size in the range $M \in [4; 297]$. The results are presented for a CIS reference (solid red), as well as for three different functionals (dashed green: CAM-B3LYP, dotted blue: B3LYP, dashed-dotted maroon: PBE). Note that the simulation with the minimal auxiliary basis, $M = 4$, already includes explicitly all states involved in the coherent dynamics. For all references presented here, the smaller bases fail to reproduce even the qualitative trends at the end of the dynamics. This indicates that the auxiliary basis is too small to describe the electronic density response and the resolution-of-identity is of poor quality. From about 50 to 186 states, the dynamics is seen

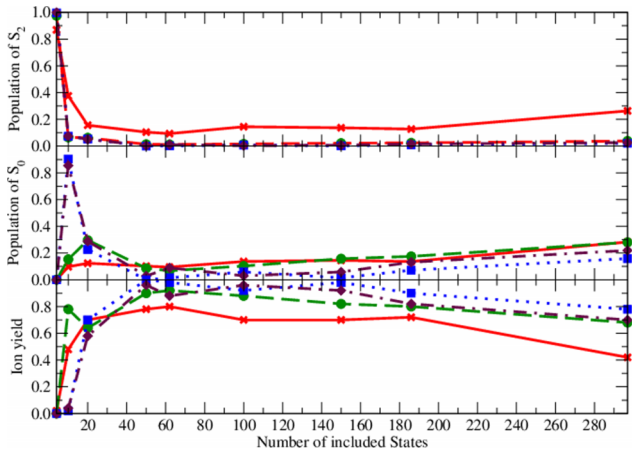

FIG. 3. Final populations of the target state (upper panel), the ground state (middle panel), and the ion yield (lower panel) for an RI-sTDCI simulation of a π-pulse excitation to S_2 based on CIS (solid red, marked with X), CAM-B3LYP (dashed green, marked with circles), B3LYP (dotted blue, marked with squares), and PBE results (dashed-dotted maroon, marked with diamonds) with increasing quality of the resolution-of-identity. The number of trajectories is set to $N_{tr} = 50$.

to have reached a plateau for all quantities shown. Beyond this largest frozen core basis, the ionization yields reduce and the bound population is distributed equally among the remaining S_0 and S_2 states. A possible explanation is that the core excitations to low-lying virtual orbitals stabilize these bound configurations by means of hole correlation, that is, via the terms of the form $\sum_{a,b}^{r} |\Psi_a^r\rangle\langle\Psi_b^r|$ that appear in the stochastic density matrix. In the reported simulations, an energetic criterion is used to select a subset of field-free Hamiltonian eigenstates, $H_{el}u_m = E_m u_m$, as a basis for the resolution-of-identity in equations of motion, Eq. (11). This choice is by no means unique. For example, selecting all eigenstates with significant contributions from excitation to bound orbitals could improve the description of hole correlation and, consequently, the dynamics beyond the frozen core approximation. As an alternative, all quasi-resonant excitations corresponding to multi-photon processes could be used instead to improve the description of the laser-molecule coupling. Despite the potentially small but non-negligible effect of dynamical hole coupling on the ionization dynamics, the subset using only 50 states is still a good approximation for the frozen core reference. Thus, this approximation will be used in all following simulations.

C. Selective laser excitation

In this section, the focus is put on the effect of the different functionals on the static properties of the molecules, and the dynamics obtained using RI-sTDCI is benchmarked against the full ρ-TDCI simulations. To this end, we performed four propagations using sTDCI with 297 configuration state functions and 50 states, averaged over 50 trajectories. The pulses tailored to drive the charge transfer dynamics are chosen to be of duration $t_p = \sigma = 200\ \frac{\hbar}{E_h}$ (4.84 fs) in all cases. The frequency is chosen resonant to the associated $S_0 \rightarrow S_2$ transition energy and the pulse amplitude is chosen according to π-pulse conditions, Eq. (17). The pulse is linearly polarized along the Cartesian axis with the largest transition dipole moment (see right panel of Fig. 4). The population of selected states obtained from the sTDCI simulation is shown in Fig. 4. At the CI Singles level, the ground state remains uncorrelated and the S_0 state is simply the Hartree-Fock (HF) configuration. The major CSF contribution to the target state S_2 state involves the transition between the orbitals depicted in the right panel. In all cases, it is the transition from a bonding orbital in the cyanide anion to an antibonding orbital between the cyanide carbon and the lithium cation. The CSF that contributes most to the target state is the HOMO – 1 → LUMO transition (for CIS, CAM-B3LYP, and PBE), except for B3LYP, where it is the HOMO – 2 → LUMO transition. As can be recognized from the shape of the orbitals involved, all excitations to the second excited state possess a strong charge transfer character.

The final population of the target state is highest for CIS (approximately 0.10), while all TDDFT references predict almost complete ionization. Among them, the CAM-B3LYP reference behaves most similarly to the CIS simulations, with a final target state population of about 0.01. The target state population at the pulse end is much lower at the PBE (about 3.5×10^{-3}) and B3LYP (~0) levels. Similar observations can be made for the ground state population dynamics: it is highest for CIS (about 0.10), and the CAM-B3LYP results (about 0.086) are closer to the CI Singles than the other functionals. In all cases, the molecule is seen to be almost completely ionized after the pulse, again with CAM-B3LYP (~0.90) providing the closest agreement with the CIS result (~0.78). The high ion yield obtained using the CAM-B3LYP and B3LYP references is due to multiphoton excitations. Indeed, the intensities of the short π-pulses used here are

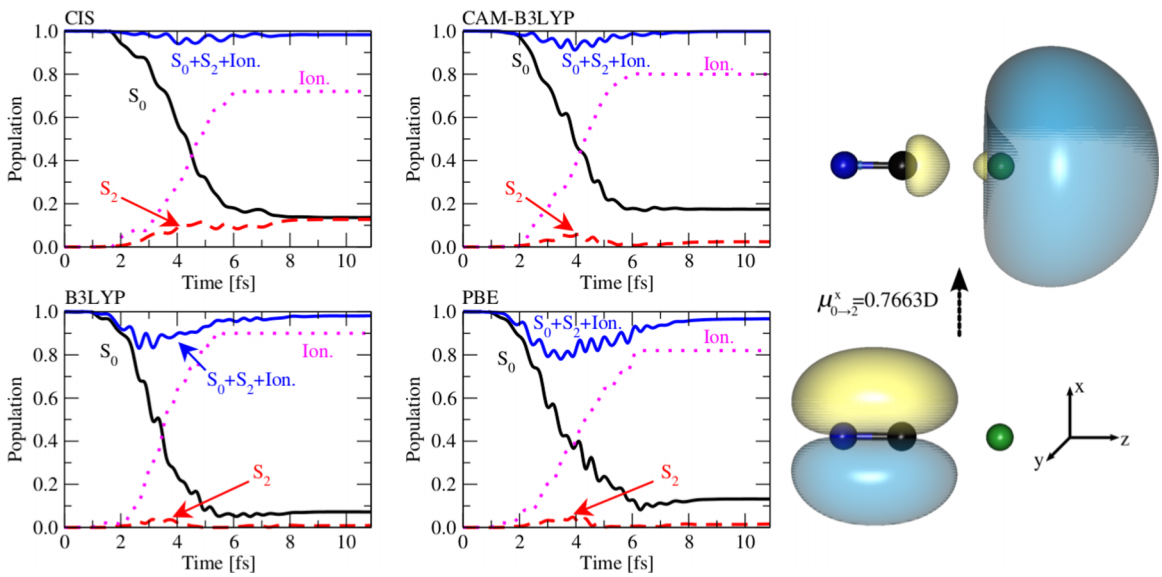

FIG. 4. Left figure: Populations of the ground state (S_0, solid black), the charge transfer state (S_2, dashed red), the ionization channel (Ion., dotted magenta), and the sum thereof ($S_0 + S_2 + Ion.$, solid blue line) during a sTDCI simulations based on CIS (upper left panel), TD-CAM-B3LYP (upper right panel), TD-B3LYP (lower left panel), and TD-PBE (lower right panel). All calculations are performed in a basis of 297 CSFs and 50 states are used for the resolution-of-identity, averaged over 50 trajectories. Right figure: dominant orbital contribution for the charge transfer state (isocontour value at $0.05 a_0^{-3/2}$). The lithium, carbon, and nitrogen atoms are, respectively, depicted in green, black, and blue.

rather high, which increases the probability of such processes. In particular, it can be seen from Fig. 1 that the two-photon process is resonant in these cases, mediating a strong coupling with the continuum. The large ionization yield in the PBE simulation finds its origin in the larger density of ionizing states at an energy close to the two-photon transition, as well as the smaller number of bound states as compared to the CIS case. The sum of ground and excited state populations and of the ion yield reveals the importance of including a large number of CSFs in the simulation to properly take into account laser-induced polarization effects. Whereas the depicted states represent the dynamics completely at the beginning and at the end of the pulse, the sum of populations is lower than one in the middle of the propagation, between 2 fs and 6 fs. This is a proof that other configurations are transiently populated as well, although not resonant with the pulse. The supplementary configurations allow for the correct description of the molecule polarizability and hyperpolarizabilities, which are included variationally to all orders in all TDCI methods. Those configurations are affected by ionization as a competing process, as the coupling with the continuum and the relaxation rates is treated as additive dissipation channels. Neglecting transient population of those intermediate configurations can lead to an erroneous description of the electron dynamics in strong laser fields.

For comparison purposes, the same laser-induced charge transfer simulations were performed using the parent method. In the ρ-TDCI formalism, the Hamilton operator is modified so as to associate an intrinsic lifetime to each CI eigenstate

$$\hat{H}_{el} \rightarrow \hat{H}_{el} - i \sum_k \Gamma_k^{(ion)} |k\rangle\langle k|, \tag{18}$$

where $|k\rangle\langle k|$ is a projector on the CI eigenstate and $\Gamma_k^{(ion)}$ is the ionization rate. Consequently, the evolution under the action of the field-free Hamiltonian is not coherent. In a first attempt, we use the model proposed above to compute the state-specific ionization rates, where restrictions are only applied through the energies of the orbitals in respective CSFs. A second one uses Klamroth's ionization scheme with a supplementary constraint on the eigenstate energies. The results for both models, based on the CIS and CAM-B3LYP references, are shown in Fig. 5. Note that here the populations of the eigenstates are shown. Interestingly, the resulting population dynamics for the model without an eigenenergy constraint are very different from those obtained from the sTDCI calculation. By the end of the propagations, no population is found in the target states and the majority of the molecules have been ionized, with the remaining population found in the ground state. As one can see from the population sum ($S_0 + S_2 + Ion.$), there is no population in other states than the ones shown in the figure and very little effect of the polarizability is seen even at the field maximum. The reason for the peculiar behavior of the target state, which reaches a higher maximum for CAM-B3LYP than for CIS, resides in

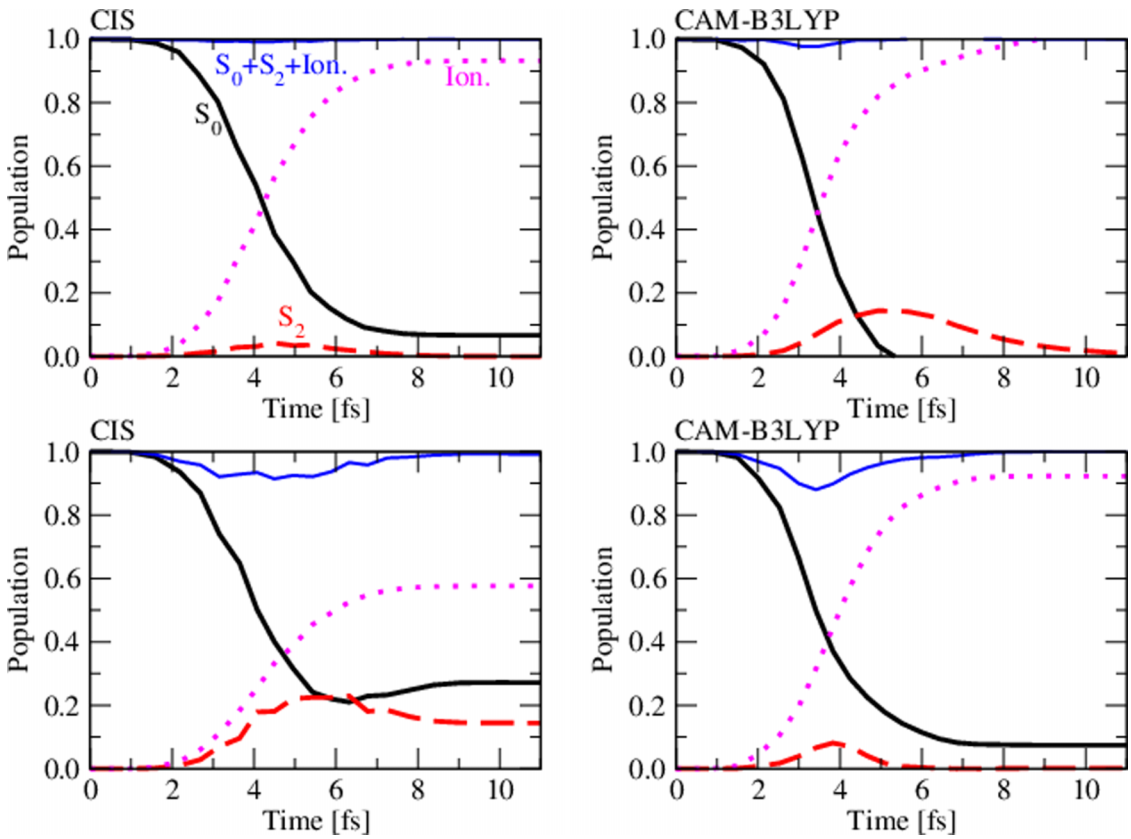

FIG. 5. Populations of the ground state (S_0, black), the second excited state (S_2, red), the ionization yield (Ion., dashed magenta), and the sum thereof ($S_0 + S_2 + Ion.$, blue) for a ρ-TDCI simulation of a resonant π-pulse excitation, based on a CIS (left panels) and TD-CAM-B3LYP (right panels) references. The present ionization model contains orbital restriction only (upper panels), and it is compared to the kinematic model of Klamroth and co-workers (lower panels). The reduced density matrix is represented using the complete basis of 297 CIS eigenstates.

the lower ionization rate of the target state in the former case ($\Gamma_2^{CAM} = 6.9 \times 10^{-3}\ \frac{E_h}{\hbar}$ vs. $\Gamma_2^{CIS} = 2.6 \times 10^{-2}\ \frac{E_h}{\hbar}$). The pulse leads to a longer-lived population of the second excited state, which ultimately decays to the ionization channel. This is an artifact of the present ionization model applied to the eigenstate basis, which constrains only the orbitals and consequently overestimates the coupling of quasi-bound eigenstates embedded in the continuum. More specifically, an ionization rate is calculated for each CSF involving a transition to a virtual orbital with a positive MO energy. Consequently, using the ρ-TDCI formalism, only the ground electronic state does not ionize for the test molecule studied here. All other states are assigned an intrinsic finite lifetime. In contrast, the RI-sTDCI ansatz considers all states used in the resolution-of-identity as bound states. Only their CSF components belonging to ionizing orbitals contribute to their decay rate, and the other CSF contributions remain bound. That means, the coupling of the eigenstates to the ionization continuum is only indirect via the CSFs, while they couple directly in the case of ρ-TDCI. In RI-sTDCI, the interaction picture Hamiltonian, Eq. (11), drives a coherent wave packet dynamics, and dephasing due to ionization and relaxation only appears when averaging over many trajectories.

Imposing the restriction that the eigenstate energies lie above the ionization threshold helps removing this artifact in the ρ-TDCI simulations. The resulting population evolutions are shown in the lower panels of Fig. 5 for the CIS and CAM-B3LYP references. In both cases, the curves show a better agreement with respect to the stochastic TDCI result, albeit not quantitatively. The population of the ground state is almost zero at the end of the pulse and the effect of electronic response at the pulse maximum can be seen from the sum population curve ($S_0 + S_2 + Ion.$). For the CIS-based simulations, the restriction on the energy reduces the ion yield since very few states in the continuum states allow for resonant two-photon processes, contrary to the CAM-B3LYP case. For the excitation probability to the ionization continuum to be large, the transition frequency must be quasi-resonant with one or more quanta excitations and have a large transition dipole moment. This is the case for CAM-B3LYP, where the $2 \rightarrow 30$ transition has an energy of 5.43 eV ($\mu^x_{2\rightarrow 27} = 0.526 ea_0$) comparable to the $0 \rightarrow 2$ transition ($\delta E_{0\rightarrow 2} = 5.40$ eV), but a larger transition dipole moment ($\mu^x_{2\rightarrow 27} = 0.526 ea_0$ vs. $\mu^x_{0\rightarrow 2} = 0.232 ea_0$, respectively). This means that, at high field intensities, population brought to target state $|2\rangle$ will preferentially absorb a second photon to reach the quasi-resonant ionizing state $|27\rangle$, which almost instantaneously decays to the continuum. A similar situation is observed for the two other functionals. In comparison, the only quasi-resonant ionizing state at the CIS levels ($\delta E_{2\rightarrow 30} = 6.46$ eV $\delta E_{0\rightarrow 2} = 6.58$ eV) is barely accessible via dipole transition ($\mu^x_{2\rightarrow 30} = 0.047 ea_0$ vs. $\mu^x_{0\rightarrow 2} = 0.302 ea_0$, respectively). Hence, in the latter case, the indirect coupling to the ionization continuum via two-photon quasi-resonant excitation is much weaker than in the TDDFT-based CI simulations.

Finally, it was demonstrated that the ionization model used in ρ-TDCI is qualitatively correct, providing a simple but sound physical interpretation for the ultrafast ionization dynamics. For example, the heuristic approach allows to accurately simulate high-harmonic generation spectra[83] and to reproduce the correct trends for ionization rates in polyenes.[62] From the comparison of Figs. 4 and 5, it should thus appear that the RI-sTDCI yields a dynamical picture of similar quality, although at only a fraction of the numerical cost. Other computationally demanding approaches using complex absorbing potentials have also been proposed[84,94,95] and might provide an even more accurate description of the ionization process.

IV. CONCLUSIONS

In conclusion, we have introduced a norm-conserving stochastic method for studying dissipative electron dynamics in presence of ionization. Both energy dissipation and ionization are represented on an equal footing using Lindblad operators with rates determined from physically motivated models, while an auxiliary continuum state describes the ionized population. Electronic response to strong field excitation with ultrashort laser pulses is treated variationally using a large basis of configuration state functions at the single excitations level, as physically simplest basis for one electron dynamical processes. This linear treatment of the field-matter interaction avoids the non-linear dependence of the time-dependent Kohn-Sham potential that plagues real-time TDDFT for strong field excitations. The representation of the operators in the interaction picture allows to the reduce numerical cost associated with the propagation by using the resolution-of-identity for the coherent part of the propagator. To improve the energetics of the zeroth-order states used in the resolution-of-identity, it is proposed to use linear response time-dependent density functional theory for the energies. The transition dipole moments required by the method are computed using the configuration interaction singles wave functions that can be obtained from a Tamm-Dancoff correspondence principle. This combination of methods can be viewed as a TDDFT-based variant of the explicitly time-dependent configuration interaction singles with perturbative corrections to the energies.

From benchmark calculations of the laser-driven charge transfer in LiCN, it is shown that the resolution-of-identity and the stochastic wave packet representation of the reduced density matrix can lead to significant numerical savings without affecting the dynamics. Comparison to reference calculations of the full reduced density matrix using the parent ρ-TDCI method reveals that the simpler model used for ionization in the RI-sTDCI captures the same physics. Finally, it is shown that the choice of reference (CIS, B3LYP, CAM-B3LYP, PBE) can affect the dynamical simulations markedly. As a rule of thumb, it can be inferred that conventional knowledge about the appropriate choice of functional for a given system can be used to guide the choice of a basis for the dynamics. For example, CAM-B3LYP should perform significantly better to describe ionization because of the better behaviour of the functional at long range. Whereas the RI-sTDCI relies on the choice of functional for the energetics involved and consequently cannot offer a better representation than the underlying functional, the linear coupling to the laser

ensures a well-behaved, variational description of electron dynamics even in strong and rapidly oscillating fields.

[1]M. Hentschel, R. Kienberger, C. Spielmann, G. A. Reider, N. Milosevic, T. Brabek, P. Corkum, U. Heinzmann, M. Drescher, and F. Krausz, Nature (London) **414**, 509 (2001).
[2]R. Kienberger, M. Hentschel, M. Uibracker, C. Spielmann, M. Kitzler, A. Scrinzi, M. Wieland, T. Westerwalbesloh, U. Kleineberg, U. Heinzmann, M. Drescher, and F. Krausz, Science **297**, 1144 (2002).
[3]M. Drescher, R. Hentschel, M. Kienberger, M. Uibracker, V. Yakovlev, A. Scrinzi, T. Westerwalbesloh, U. Kleineberg, U. Heinzmann, and F. Krausz, Nature (London) **419**, 803 (2002).
[4]P. H. Bucksbaum, Nature (London) **421**, 593 (2003).
[5]G. G. Paulus, F. Lindner, H. Walther, A. Baltuka, E. Goulielmakis, M. Lezius, and F. Krausz, Phys. Rev. Lett. **91**, 253004 (2003).
[6]J. Itatani, J. Levesque, D. Zeidler, H. Niikura, H. Pépin, J. C. Kieffer, P. B. Corkum, and D. M. Villeneuve, Nature (London) **432**, 867 (2004).
[7]A. Föhlisch, P. Feulner, F. Hennies, D. Fink, A. Menzel, P. M. Sanchez-Portal, D. Echenique, and W. Wurth, Nature (London) **436**, 373 (2005).
[8]M. F. Kling, C. Siedschlag, A. J. Verhoef, J. I. Khan, M. Schultze, T. Uphues, Y. Ni, M. Uiberacker, M. Drescher, F. Krausz, and M. J. J. Vrakking, Science **312**, 246 (2006).
[9]F. Krausz and M. Y. Ivanov, Rev. Mod. Phys. **81**, 163 (2009).
[10]M. Dantus, M. J. Rosker, and A. H. Zewail, J. Chem. Phys. **87**, 2395 (1987).
[11]T. S. Rose, M. J. Rosker, and A. H. Zewail, J. Chem. Phys. **88**, 6672 (1988).
[12]P. B. Corkum and F. Krausz, Nat. Phys. **3**, 381 (2007), and references therein.
[13]H. J. Wörner, J. B. Bertrand, D. V. Kartashov, P. B. Corkum, and D. M. Villeneuve, Nature (London) **466**, 604 (2010).
[14]K. Kulander, Phys. Rev. A **36**, 2762 (1987).
[15]R. Grobe and J. H. Eberly, Phys. Rev. A **48**, 4664 (1993).
[16]M. Pindzola, P. Gavras, and T. Gorczyca, Phys. Rev. A **51**, 3999 (1995).
[17]H. Yu and A. Bandrauk, Phys. Rev. A **56**, 685 (1997).
[18]F. Remacle and R. Levine, J. Chem. Phys. **110**, 5089 (1999).
[19]F. Calvayrac, P.-G. Reinhard, E. Suraud, and C. Ullrich, Phys. Rep. **337**, 493 (2000).
[20]K. Harumiya, I. Kawata, H. Kono, and Y. Fujimura, J. Chem. Phys. **113**, 8953 (2000).
[21]J. Breidbach and L. Cederbaum, J. Chem. Phys. **118**, 3983 (2003).
[22]M. Suzuki and S. Mukamel, J. Chem. Phys. **119**, 4722 (2003).
[23]T. Klamroth, Phys. Rev. B **68**, 245421 (2003).
[24]S. Laulan and H. Bachau, Phys. Rev. A **68**, 013409 (2003).
[25]J. Zanghellini, M. Kitzler, C. Fabian, T. Brabec, and A. Scrinzi, Laser Phys. **13**, 1064 (2003).
[26]T. Kato and H. Kono, Chem. Phys. Lett. **392**, 533 (2004).
[27]X. Chu and S. I. Chu, Phys. Rev. A **70**, 61402 (2004).
[28]G. Paramonov, Chem. Phys. Lett. **411**, 305 (2005).
[29]T. Burnus, M. Marques, and E. K. U. Gross, Phys. Rev. A **71**, 010501 (2005).
[30]M. Nest, T. Klamroth, and P. Saalfrank, J. Chem. Phys. **122**, 124102 (2005).
[31]P. Krause, T. Klamroth, and P. Saalfrank, J. Chem. Phys. **123**, 074105 (2005).
[32]P. Krause, T. Klamroth, and P. Saalfrank, J. Chem. Phys. **127**, 034107 (2007).
[33]I. Barth and J. Manz, Angew. Chem., Int. Ed. **45**, 2962 (2006).
[34]I. Barth, J. Manz, Y. Shigeta, and K. Yagi, J. Am. Chem. Soc. **128**, 7043 (2006).
[35]T. Klamroth, J. Chem. Phys. **124**, 144310 (2006).
[36]A. Castro, M. Marques, H. Appel, M. Oliveira, C. Rozzi, X. Andrade, F. Lorenzen, E. K. U. Gross, and A. Rubio, Phys. Status Solidi B **243**, 2465 (2006).
[37]H. Schlegel, S. Smith, and X. Li, J. Chem. Phys. **126**, 244110 (2007).
[38]B. Schäfer-Bung and M. Nest, Phys. Rev. A **78**, 012512 (2008).
[39]J. Schmidt, E. Goulielmakis, and V. S. Yakovlev, J. Phys. B: At., Mol. Opt. Phys. **41**, 115602 (2008).
[40]J. C. Tremblay, T. Klamroth, and P. Saalfrank, J. Chem. Phys. **129**, 084302 (2008).
[41]S. Klinkusch, T. Klamroth, and P. Saalfrank, Phys. Chem. Chem. Phys. **11**, 3875 (2009).
[42]S. Klinkusch, P. Saalfrank, and T. Klamroth, J. Chem. Phys. **131**, 114304 (2009).
[43]T. Klamroth and M. Nest, Phys. Chem. Chem. Phys. **11**, 349 (2009).
[44]M. Nest, Chem. Phys. Lett. **472**, 171 (2009).
[45]J. C. Tremblay, S. Klinkusch, T. Klamroth, and P. Saalfrank, J. Chem. Phys. **134**, 044311 (2011).
[46]S. Klinkusch and T. Klamroth, J. Theor. Comput. Chem. **12**, 1350005 (2013).
[47]H. Miyagi and L. B. Madsen, Phys. Rev. A **87**, 062511 (2013).
[48]H. Miyagi and L. B. Madsen, Phys. Rev. A **89**, 063416 (2014).
[49]S. Bauch, L. K. Sørensen, and L. B. Madsen, Phys. Rev. A **90**, 062508 (2014).
[50]E. Runge and E. K. U. Gross, Phys. Rev. Lett. **52**, 997 (1984).
[51]S. Raghunathan and M. Nest, J. Chem. Theory Comput. **7**, 2492 (2011).
[52]S. Raghunathan and M. Nest, J. Chem. Theory Comput. **8**, 806 (2012).
[53]S. Raghunathan and M. Nest, J. Chem. Phys. **136**, 064104 (2012).
[54]I. Shavitt, Int. J. Quantum Chem. **S11**, 131 (1977).
[55]I. Shavitt, in *Methods of Electronic Structure Theory*, edited by H. F. Schäfer (Plenum, New York, 1977).
[56]C. Huber and T. Klamroth, Appl. Phys. A **81**, 91 (2005).
[57]P. Saalfrank, T. Klamroth, C. Huber, and P. Krause, Isr. J. Chem. **45**, 205 (2005).
[58]P. Krause and T. Klamroth, J. Phys. Chem. **128**, 234307 (2008).
[59]P. Horsch, G. Urbasch, K.-M. Weitzel, and D. Kröner, Phys. Chem. Chem. Phys. **13**, 2378 (2011).
[60]R. Ramakrishnan, S. Raghunathan, and M. Nest, Chem. Phys. **420**, 44 (2013).
[61]A. D. Dutoi, Mol. Phys. **112**, 1 (2014).
[62]J. A. Sonk and H. B. Schlegel, J. Phys. Chem. A **116**, 7161 (2012).
[63]K. Blum, *Density Matrix Theory and Applications* (Plenum Press, New York, 1996).
[64]J. C. Tremblay, P. Krause, T. Klamroth, and P. Saalfrank, Phys. Rev. A **81**, 063420 (2010).
[65]J. C. Tremblay, J. Chem. Phys. **134**, 174111 (2011).
[66]N. Gisin and I. C. Percival, J. Phys. A: Math. Gen. **25**, 5677 (1992).
[67]J. Dalibard, Y. Castin, and K. Molmer, Phys. Rev. Lett. **68**, 580 (1992).
[68]R. Dum, P. Zoller, and H. Ritsch, Phys. Rev. A **45**, 4879 (1992).
[69]H. Carmichael, in *An Open Systems Approach to Quantum Optics*, edited by H. Araki (Springer-Verlag, Berlin, 1993).
[70]K. Molmer, Y. Castin, and J. Dalibard, J. Opt. Soc. Am. B **10**, 524 (1993).
[71]N. Gisin and I. C. Percival, J. Phys. A: Math. Gen. **26**, 2245 (1993).
[72]H.-P. Breuer and F. Petruccione, Phys. Rev. E **51**, 4041 (1995).
[73]M. B. Plenio and P. L. Knight, Rev. Mod. Phys. **70**, 101 (1998).
[74]P. Saalfrank, Chem. Phys. **211**, 265 (1996).
[75]H.-P. Breuer and F. Petruccione, *The Theory of Open Quantum Systems* (Oxford University Press, Oxford, 2006).
[76]L. Greenman, P. J. Ho, S. Pabst, E. Kamarchik, D. A. Mazziotti, and R. Santra, Phys. Rev. A **82**, 023406 (2010).
[77]M. Awasthi, Y. V. Vanne, and A. Saenz, J. Phys. B: At., Mol. Opt. Phys. **38**, 3973 (2005).
[78]R. Paunz, *Spin Eigenfunctions* (Plenum, New York, 1979).
[79]J. Whitten, J. Chem. Phys. **58**, 4496 (1973).
[80]E. Baerends, D. Ellis, and P. Ros, Chem. Phys. **2**, 41 (1973).
[81]B. Dunlap, J. Connolly, and J. Sabin, J. Chem. Phys. **71**, 3396 (1979).
[82]O. Vahtras, J. Almlöf, and M. Feyereisen, Chem. Phys. Lett. **213**, 514 (1993).
[83]A. White, C. Heide, P. Saalfrank, M. Head-Gordon, and E. Luppi, Mol. Phys. **114**, 947 (2016).
[84]N. Rohringer, A. Gordon, and R. Santra, Phys. Rev. A **74**, 043420 (2006).
[85]P. C. Hariharan and J. A. Pople, Theor. Chim. Acta **28**, 213 (1973).
[86]M. W. Schmidt, K. K. Baldridge, J. A. Boatz, S. T. Elbert, M. S. Gordon, J. J. Jensen, S. Koseki, N. Matsunaga, K. A. Nguyen, S. J. Su, T. L. Windus, M. Dupuis, and J. A. Montgomery, J. Comput. Chem. **13**, 1347 (1993).
[87]J. P. Perdew, K. Burke, and M. Ernzerhof, Phys. Rev. Lett. **77**, 3865 (1996).
[88]J. P. Perdew, K. Burke, and M. Ernzerhof, Phys. Rev. Lett. **78**, 1396 (1997).
[89]T. Yanai, D. Tew, and N. Handy, Chem. Phys. Lett. **393**, 51 (2004).
[90]A. D. Becke, Phys. Rev. A **38**, 3098 (1988).
[91]C. Lee, W. Yang, and R. G. Parr, Phys. Rev. B **37**, 785 (1988).
[92]B. Miehlich, A. Savin, H. Stoll, and H. Preuss, Chem. Phys. Lett. **157**, 200 (1989).
[93]T. C. Koopmans, Physica (Amsterdam) **1**, 104 (1934).
[94]P. Krause, J. Sonk, and H. Schlegel, J. Chem. Phys. **140**, 174113 (2014).
[95]P. Krause and H. Schlegel, J. Phys. Chem. Lett. **6**, 2140 (2015).